ADVANCED OPTICAL MATERIALS

Supporting Information

for *Advanced Optical Materials,* DOI: 10.1002/adom.201700923

Through the Spherical Looking-Glass: Asymmetry Enables Multicolored Internal Reflection in Cholesteric Liquid Crystal Shells

Yong Geng, Ju-Hyun Jang, Kyung-Gyu Noh, JungHyun Noh, Jan P. F. Lagerwall, and Soo-Young Park**

Supporting Information

Through the spherical looking-glass: asymmetry enables multicolored internal reflection in cholesteric liquid crystal shells

Yong Geng[1,+], Ju-Hyun Jang[2,+], Kyung-Gyu Noh[2], JungHyun Noh[1], Jan Lagerwall[1,*], and Soo-Young Park[2,*]

SI Materials and Methods

We prepared two cholesteric liquid crystal (ChLC) mixtures for this study. ChLC1 has a pitch that is largely temperature independent. It is composed of the commercial nematic liquid crystal mixture RO-TN 615 (Roche, Switzerland) and the chiral dopant R-811 (Merck, Germany). The ChLC pitch can be tuned as desired by varying the concentration of the chiral dopant. We explored the range from 20 to 28 wt.-%, corresponding to normal incidence selective reflection color from infrared to yellow-green.

ChLC2 has relatively strong temperature dependence of the pitch length, allowing tunability of normal incidence selective reflection color from yellow to red by changing the temperature from 30 to 60°C. This mixture was prepared by adding 35 wt.-% of the chiral dopant (S)-4-cyano-4'-(2-methylbutyl)biphenyl, CB15 (Synthon, Germany), to the non-chiral nematic liquid crystal host MLC-2132 (Merck, UK).

In order to stabilize the ChLC shells and prevent the shells from collapsing, we added water-soluble polymer, polyvinylalcohol (PVA) to the inner and outer isotropic phases: PVA (Mw 13,000 - 23,000 g mol^{-1}, 88-89% hydrolyzed, Sigma-Aldrich) was used for shells from ChLC1 and PVA from a different supplier (Product number #1500 from Yakuri, Japan) was used for shells from ChLC2.

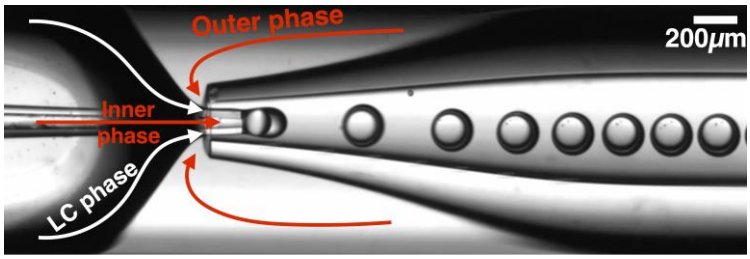

Figure S1: Shell production using a glass capillary microfluidic set-up. The production was done at about 60°C (above the clearing temperature of the ChLC), to reduce the viscosity of the liquid crystal mixture.

To promote asymmetric shells of different types (thinner at top and thicker at bottom, or vice versa) we tuned the density of the inner isotropic phase, by changing its

composition, to be lower or higher than that of the ChLC. The same isotropic liquid was used for the outer phase. A less dense isotropic phase was achieved by using pure water to which was added 5 wt.-% PVA. As described and explained in the main paper, the shells were close to symmetric right after the shell production, despite the lower density inner phase, but over the course of about two weeks the shells reached their equilibrium configuration, becoming highly asymmetric with very thin top part and rather thick bottom. If the opposite asymmetry was desired, (thinner at the shell bottom and thicker at the top), 50 vol.-% of glycerol was added to the aqueous PVA solution forming the inner and outer phases. Perfect density matching is very di cult to achieve, not least because the densities of the ChLC and the inner droplet exhibit non-identical temperature dependencies. Further complications arise from the non-negligible miscibility of glycerol with the LC[1] and the variations in LC density as the chiral dopant concentration is changed to tune the helix pitch. For the two types of ChLC used in the study, density matching of the aqueous phase was approached with about 18% (ChLC2) and 10% (ChLC1) glycerol, respectively. All shells were produced in nested glass capillary microfluidic devices, following the basic principle of Utada et al.[2]. Cylindrical glass capillaries (Victrocom, USA, 0.7 mm inner diameter, 0.87 mm outer diameter) were tapered in half using a micropipette puller (P-100, Sutter instrument, USA), the end cut of with a microforge (Narishige, Japan) to create the orifice with defined size. One tapered capillary was used for injection of the inner aqueous phase into the LC phase, the other was used as collection tube. The two tapered cylindrical capillaries were inserted, with their orifices facing each other, into a capillary with square cross section (Victrocom, USA, 0.9 mm inner side length, 0.18 mm wall thickness), the inner side length matched to the outer diameter of the cylindrical capillaries. The LC was flowed through the corners of the square capillary along the injection capillary flow, the outer phase was flowed in the same capillary in the opposite direction from the other side. When these two immiscible phases meet close to the two cylindrical capillary orifices, flow focusing of the LC, with encapsulated inner phase, into the outer phase results if all three flow speeds are optimized[2], Fig. S1.

The outer surface of the injection capillary and the inner surface of the collection capillary were treated using octadecyl trichlorosilane (Sigma-Aldrich) and 3-[methoxy (polyethyleneoxy) propyl] trimethoxysilane (90%, 6-9 PE units) (ABCR GmbH), respectively, to ensure hydrophobic and hydrophilic characteristics for these two interfaces. The outer square capillary was left untreated.

The shell production was monitored using an NX4-S3 (Integrated Design Tools, Inc.) high-speed video camera mounted on a Nikon Eclipse TS100 inverted microscope. The microfluidic set-up was mounted in a heating stage for ensuring that the ChLC was in the isotropic phase during production.

For optical microscopy characterization, we filled the shell suspension into a flat glass capillary and sealed the openings to keep the sample stable over several weeks. The shells were investigated in a polarizing microscope (Olympus BX51, Japan) equipped with a digital camera (Olympus DP73, Japan). All reflection observations were done with fully closed aperture diaphragm.

S2 Microscopy along and perpendicular to gravity

We use two different observation modes in optical microscopy. Fig. S2a shows schematically how a shell is observed along the direction of gravity, which is the standard geometry in microscopy. This does not allow a direct assessment of the shell asymmetry, as induced by buoyancy, a critical parameter for the analysis of the optical properties of the shell. In order to assess the shell asymmetry, we fix the sample inside a hot stage which is mounted securely on the microscope stage, via an xy-translator. A video camera is mounted on the microscope for continuous sample observation. We then tilt the whole set-up by 90^{o} , as illustrated in Fig. S2b. The camera now shows the shells from the side, perpendicular to the direction of gravity. Since the change in gravitational force direction sets the shells in motion, the xy translator is used to track the shells until they reach steady state at the new top or bottom of the capillary (previously the side). Movie. S1 was obtained with the microscope in this orientation.

S3 Reduced shell symmetry by heating the shells to the isotropic phase

To corroborate if the nearly symmetric shell geometry even in non-density matched shells is due to the liquid crystal phase, we heat the liquid crystal shell at 20 K min^{-1} from 30℃ to the isotropic phase at 60℃, Fig. S3. To fully confirm shell asymmetry, we tilt the microscope to 90^{o} prior to heating the sample. Fig. S3b shows a nearly symmetric shell at 30℃ in the cholesteric phase, observed from the side in the tilted geometry. The shell shows no noticeable change in character throughout the cholesteric phase range, but once the shell goes isotropic at 60℃ (the clearing point) the inner droplet, slightly lighter than the liquid crystal, starts to move up. Fig. S3c shows the shell immediately after the clearing transition. The heating is now stopped and we keep the temperature at 60℃. Within about 2 minutes the inner drop has reached very close to the top, due to buoyancy, leaving only a very thin liquid crystal layer between inner and outer phases at this point, see Fig. S3d. This experiment confirms that the short-pitch cholesteric liquid crystal phase initially promotes symmetry, acting against buoyancy. (See also Movie. S1)

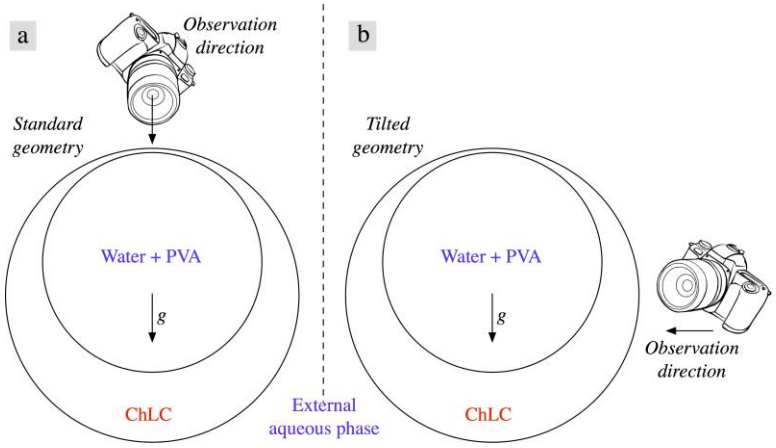

Figure S2: Schematic drawings of the two observation modes employed: (a) observation is done along gravity, as in standard optical microscopy. (b) the shell is filmed in a

direction perpendicular to gravity, achieved by tilting the microscope to90°.

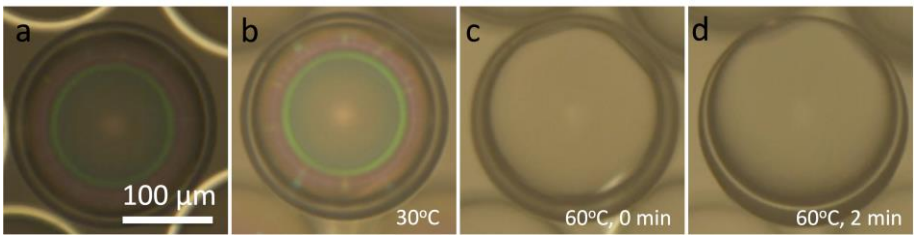

Figure S3: Transmission microscopy images (no polarizers) of shells while heating to the isotropic phase: (a) the shell is seen along the gravity direction in the standard geometry (shown in Fig. S2a), (b-d) Side view of the shell in the tilted geometry (drawn in Fig. S2b) with the direction of gravity being from top to bottom of the page; (b) The shell imaged in (a) turns out to be nearly symmetric in thickness at 30℃, and it remains so until (c), when the temperature reaches 60℃ and the shell goes to the isotropic phase. In (d) the same shell is seen 2 minutes later, after keeping it at 60℃. The shell is now strongly asymmetric, with very thin top, due to the effect of buoyancy. (Snapshots taken from Movie. S1)

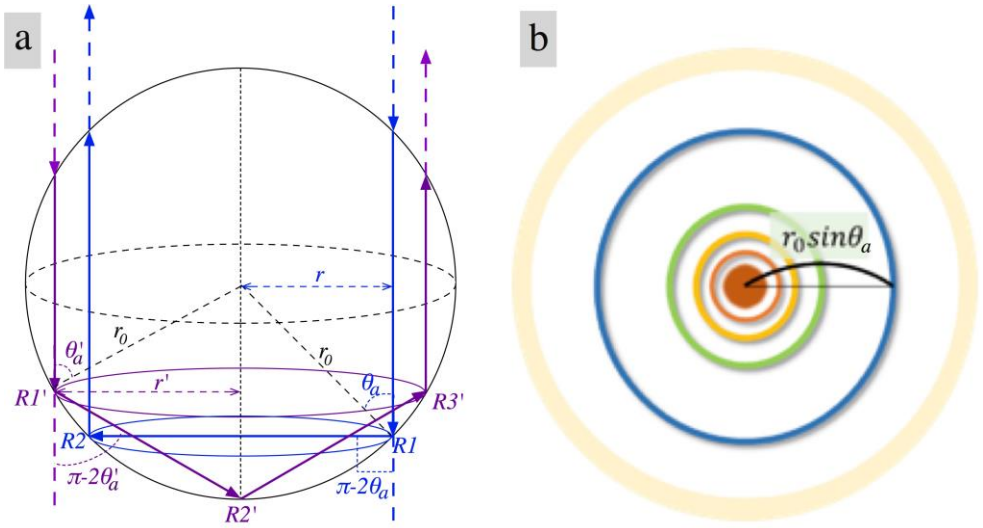

Figure S4: Schematic drawings of a shell of ChLC and the internal reflection process: (a) cross sectional perspective and (b) top views. In (a), two ring-generating internal reflection paths have been drawn, for $n = 2$ and $n = 3$ internal reflection points, respectively. Drawing (b) shows the colors of the rings from above, assuming a normal selective reflection color (central spot) in the red regime. The radius of each ring is calculated as $r_0 \sin\theta_a$, where r_0 is the radius of the inner droplet and θ_a is the apparent angle of incidence inside the aqueous phase for the reflections giving rise to the ring.

S4 Calculation of internal reflection ring parameters

We now present a detailed analysis of the internal reflection ring parameters. Fig. S4a

shows a simple scheme, considering two ring-generating paths in opposite directions, with two and three internal reflection events, respectively. One path is indicated with blue arrows, representing a blue visible ring generated by a ChLC that reflects at $\lambda_N = 620\ nm$ along the helix. The other path is drawn with violet arrows. The ring generated through this path is not visible to the human eye, as its wavelength lies in the ultraviolet region. For both paths we assume, for simplicity, a vertical initial ray direction of the white light that has entered the inner droplet from above (only the inner shell interface, between inner droplet and ChLC, is drawn in Fig. S4a).

The incident white light hits the bottom inside shell interface at points *R*1 and *R*1', with apparent incidence angles θ_a and θ'_α, respectively, and the ChLC then reflects the blue and ultraviolet components of the two respective rays within the inner droplet. At each reflection, the propagation direction of the blue ray changes by the angle $\pi - 2\theta_a$and the same relation holds for the UV ray, as indicated in the figure. The same type of reflection takes place at other points, once (blue ray) or twice (UV ray) inside the shell, with the same incidence angle, as the reflections take place within a sphere.

Table S1: Reduced radii r/r_0 of the internal reflection rings as a function of m and n, as established by equation [3].

n	***r/r$_0$@m=1***	***r/r$_0$@m=3***	***r/r$_0$@m=5***	***r/r$_0$@m=7***
2	0.70711			
3	0.86603			
4	0.92388	0.38268		
5	0.95106	0.58779		
6	0.96593	0.70711	0.25882	
7	0.97493	0.78183	0.43388	
8	0.8079	0.83147	0.55557	0.19509
9	0.98481	0.86603	0.64279	0.34202
10	0.98769	0.89101	0.70711	0.45399
11	0.98982	0.90963	0.75575	0.54064
12	0.99144	0.92388	0.7933	0.60876

The total number of reflection events inside the shell is two and three, respectively, in the depicted cases (Fig. S4a). As shown in Fig. 3 in the main paper, there can be many more. In order for the observer to see the reflected light, the ray must eventually be sent back up vertically (to make the problem tractable we here ignore the non-zero numerical aperture (NA) of the objective used for imaging; as discussed in the main paper and below, this must be taken into account to fully understand all observations), i.e. the total rotation that the ray has experienced as a result of reflections in the shell must be $m\pi$, where m is an odd integer (m = 1, 3, 5, . . .). For simplicity we ignore the refraction as the ray passes through the shell (a simplification that in this case becomes more acceptable due to the non-zero NA; since the refractive index differences between ChLC and isotropic phases are not very large, a ray that leaves the inner droplet with a vertical direction prior to exit will certainly be imaged). Generalizing the model to an arbitrary number *n* of internal reflections, with corresponding generalized apparent angle of incidence θ_a the following relations are formulated:

$$m\pi = n(\pi - 2\theta_a) \tag{1}$$

$$\theta_a = \frac{(n-m)\pi}{2n} \tag{2}$$

Equation (2) tells us which apparent incidence angles θ_a are possible for giving rise to a visible internal selective reflection ring. Based on the geometrical relations in Fig. S4a, we can then calculate the radius r of each internal reflection ring (defined by *m*, *n*) using the expression for the allowed angles θ_a:

$$r_{mn} = r_0 \sin\theta_a = r_0 \sin\frac{(n-m)\pi}{2n} \tag{3}$$

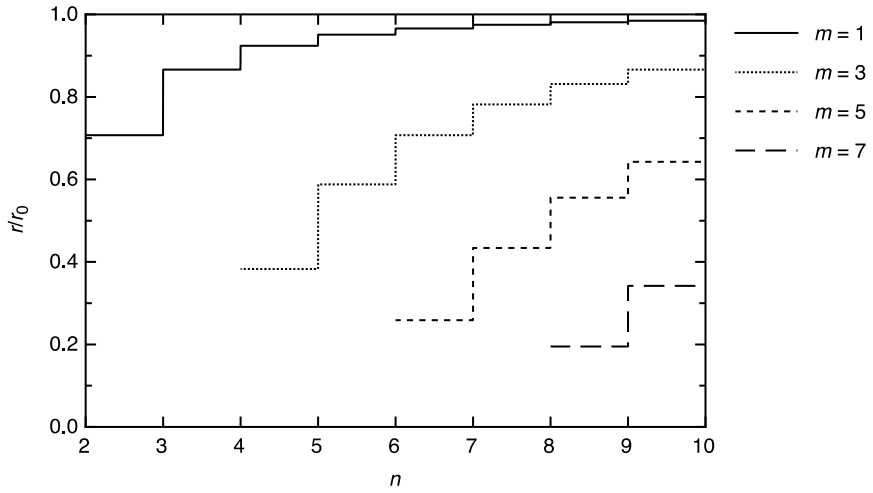

Figure S5: The reduced reflection ring radius (ring radius *r* normalized by the shell radius r_0) as a function of number of internal reflections *n* and the number *m* of ray

direction reorientations by π, as calculated from equation [3].

where r_0 is the radius of the inner shell. Using equation (3) we plot the reduced radii r/r_0 as a function of n (up to 10) for the first four values of m in Fig. S5, and we tabulate the reduced radii for $m = 1,3,5,7\ and\ n = 2\ to 12$ in table S1. By measuring the ring radius and normalizing it by the inner shell radius we can establish which combinations of *m* and *n* give rise to a certain ring, see Fig. 4 in the main manuscript and Fig. S9. Equation (3) and Fig. S5 show that, for the same value of *m*, the ring must be larger the larger the number n of internal reflection events. Because equation (2) tells us that greater n means greater apparent incidence angle θ_a, we can verify this result experimentally by studying the color of each ring, since the angle of incidence determines the reflection wavelength through Bragg's law:

$$\lambda_\theta = \lambda_N \cos\theta = \bar{n}_{Ch} p \cos(\theta) \tag{4}$$

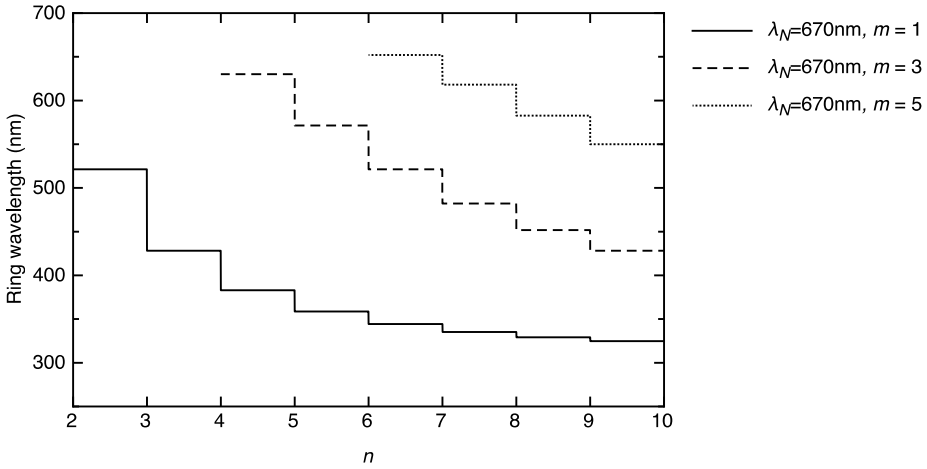

Figure S6: The wavelengths of the internal reflection rings as a function of number of internal reflections n and the number *m* of ray direction reorientations by π, as calculated from equation [6] for the case of a cholesteric giving normal incidence reflection at $\lambda_N \approx 650\ nm$ and assuming refractive indices n_{aq} = 1.35 and $\bar{n}_{Ch}$ = 1.52.

Here λ_N is wavelength at normal incidence reflection (along the helix, $\theta = 0$), $\bar{n}_{Ch}$is the average refractive index of the ChLC, and *p* is the pitch length. The bandwidth is $\Delta\lambda = \Delta n p$, where Δn is the (local; ignoring the helical modulation) birefringence of the ChLC. We now need to formulate the angle of incidence *within* the cholesteric, with respect to

the helix axis, θ, as a function of the apparent reflection angle θ_a in the internal aqueous phase. This relation is given by Snell's law, stating that:

$$n_{aq} \sin\theta_a = \bar{n}_{Ch} \sin\theta \Longrightarrow \theta = arc\ sin \frac{n_{aq}}{\bar{n}_{Ch}} \sin\theta_a \quad (5)$$

where n_{aq} is the refractive index of the internal isotropic aqueous phase. Inserting equation (2) into (4), using equation (5), we obtain a formal expression for the central wavelength of each ring, complementing equation (3) for the ring radius:

$$\lambda_{mn} = \bar{n}_{Ch} p \cos(arc\sin(\frac{n_{aq}}{\bar{n}_{Ch}} \sin\frac{(n-m)\pi}{2n})) \quad (6)$$

The ring wavelengths predicted by equation (6) are plotted for $n = 2\ to\ 10$ and $m = 1,3,5$ in Fig. S6 for the case of $\lambda_N = 670\ nm$. In the main paper, Fig. 3 shows 12 possible ring-generating light paths inside the shell, with rays drawn in the expected colors considering the same $\lambda_N = 670\ nm$ (except for *m = 1, n > 3*, which yield UV reflection), established by the calculations above.

Let us finally extract the angular argument from equation [3]:

$$\frac{(n-m)\pi}{2n} = arcsin\frac{r}{r_0} \quad (7)$$

and insert the result in equation [6] for the reflection wavelength (using $\lambda_N = \bar{n}_{Ch} p$), to get a direct relation between reflection color and ring radius:

$$\lambda_r = \lambda_N \cos(\arcsin(\frac{n_{aq}}{\bar{n}_{Ch}} \frac{r}{r_0})) \quad (8)$$

While this relation is very convenient, as it shows directly how the ring color must change with diameter for each value of λ_N, one must remember that we lose the restrictions on *m* and *n*. This may give the false impression that any color and any ring diameter would be possible. In the plot of equation (8) (Fig. S7) we have therefore indicated a few possible reduced ring diameters with vertical dashed lines, each labeled with the corresponding values of n and m, to remind which combinations of reflection wavelength and ring diameter are actually possible.

The above analysis is in general supported by our experimental observations, as in most cases the ring wavelength gets smaller the greater the ring diameter. As mentioned in the main manuscript, the exception is the weak green ring appearing outside the outermost blue ring in shells with $\lambda_N \approx 650\ nm$. This anomalous (from the point of view of our model) ring demonstrates the limitations of our model. The requirement of vertical input and exit directions makes the analysis tractable, but in reality the non-zero numerical

aperture (NA) of the microscope objective means that the shell is illuminated with a cone of light rays, and the imaging collects all light that enters the objective within a certain cone angle, defined by NA. The weak green ring that does not fit into our model is most likely a result of such a light path with non-vertical exit ray, which is nevertheless close enough to vertical that the microscope objective images it.

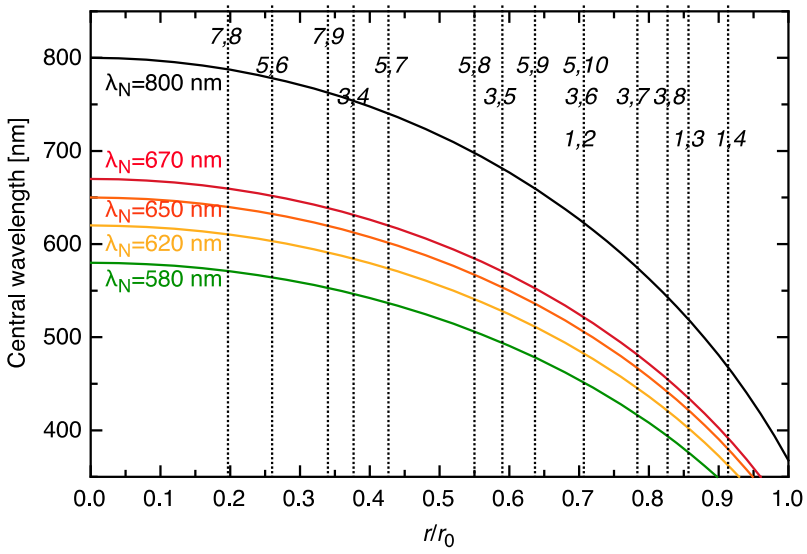

Figure S7: The wavelengths of the internal reflection rings as a function of the reduced radius r/r_0, for 4 values of the normal incidence reflection wavelength λ_N, assuming refractive indices n_{aq} = 1.35 and $\bar{n}_{Ch}$ = 1.52. Note that the curves are false in the sense that only certain combinations of reflection wavelength and reduced radius fulfill the criteria for back reflection. Some of the possible combinations of *m* and *n* have been indicated with vertical dashed lines.

S5 Color sequence of internal reflection rings is independent of shell diameter and thickness

In the above geometrical analysis, the diameter and thickness of the shell do not enter in the expressions for the color of the rings, hence these parameters should have no impact on the ring colors or the color sequence. To experimentally confirm this hypothesis, we prepared shells from the ChLC2 mixture with different diameter ($2r_0$) and thickness (t). From left to right in Fig. S8, the inner diameters of the shells are gradually increasing, and at the same time, the shell thickness increases as well. In all cases, the shell texture appears to be the same with four clearly visible concentric reflection rings in

the color sequence orange, yellow, green, and blue, from the center outwards. This confirms that the reflection ring color is not dependent on the shell size and thickness, but only on the ChLC pitch, the radius of the reflection ring and the refractive index ratio $\frac{n_{aq}}{\bar{n}_{Ch}}$. Table S2 summarizes the analysis of the three shells using the above analytical model.

Table S2: Experimental data on internal reflection rings from the ChLC shells in Fig. S8 ($\lambda_N \approx 620\ nm$; ring nr. counts from inside outwards).

ChLC shell	**Ring nr.**	**Ring color**	**Ring radius *r* *[μm]***	***r/r*$_0$**	***m,n***
Fig.S8a	1	Orange	29.5	0.199	7,8
	2	Yellow	8.6	0.260	5,6
	3	Green	356.8	0.384	3,4
	4	Blue	104.9	0.708	1,2/3,6
Fig.S8b	1	Orange	32.4	0.193	7,8
	2	Yellow	43.4	0.258	5,6
	3	Green	64.8	0.385	3,4
	4	Blue	118.5	0.705	1,2/3,6
Fig.S8c	1	Orange	38	0.197	7,8
	2	Yellow	50.1	0.260	5,6
	3	Green	74	0.385	3,4
	4	Blue	136	0.708	1,2/3,6

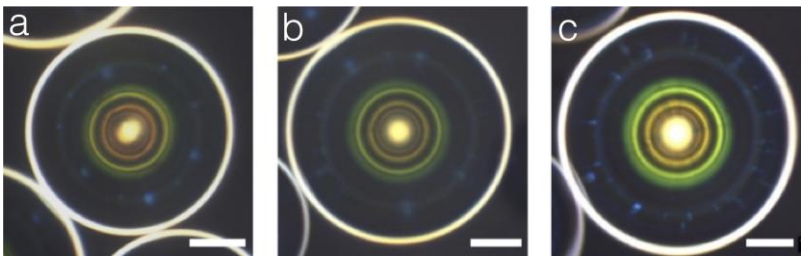

Figure S8: Reflection microscopy (no polarizers) images of shells of ChLC, reflecting

orange light ($\lambda_N \approx 620\,nm$) at normal incidence, with increasing inner shell diameter ($2r_0$) and average shell thickness (t) from left to right. The measured values for $2r_0$ and *t*, respectively, are (a) 150 μm, 9 μm, (b) 170 μm, 10 μm, and (c) 190 μm, 13 μm. All scale bars are 100 μm.

S6 Mixture composition- based tuning of the internal reflection ring wavelengths

Using a shell of the temperature-responsive mixture ChLC2, we showed that the wavelength of the internal reflection rings can be tuned by changing the cholesteric pitch *p* in Fig. 7 in the main paper. Here we also confirm the phenomena with shells from various compositions of the less temperature-sensitive mixture class ChLC1. By preparing three mixtures, containing the chiral dopant at concentrations 28, 24 and 20 wt.-%, respectively, we produced shells reflecting yellow-green, red and infrared at normal incidence, respectively (Fig. S9). As expected, the increasing pitch as the concentration of chiral dopant is reduced, is reflected by a red-shift of all internal selective reflection rings. Comparing the short-pitch mixture in Fig. S9a with the long-pitch mixture in Fig. S9c we see that we can optimize the visibility of small and large rings, respectively by choosing short or long pitch of the ChLC. For the intermediate pitch value in Fig. S9b we measured the reduced ring radii and identified their respective m, n values, as indicated in the figure.

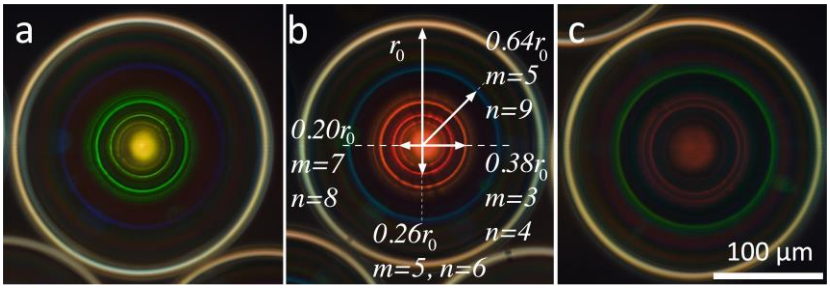

Figure S9: Reflection polarizing microscopy (right-handed circular polarizer and analyzer) images of internal reflection rings from shells of ChLC1 with increasing pitch from left to right (normal reflection color yellow-green, red and infrared, respectively). For the shell in (b) the rings have been indexed according to their reduced radii r/r_0 and the respective *m*, *n* values are indicated.

S7 Analysis of selective reflection patterns with different polarization settings.

We finally verify the polarization of the colorful internal selective reflection rings as well as of the white light that experienced total internal reflection (TIR) within the

actual LC shell (see main paper). In Fig. S10, a few shells of the ChCL1 mixture class with varying concentrations of chiral dopant, and thus varying pitch, are investigated in reflection with illumination from above. In Fig. S10a the shells are illuminated by right-handed circular polarized light and they are observed through a right-handed circular analyzer (effectively $\lambda/4$ plate followed by linear polarizer, in appropriate relative configuration) resulting in internal reflection rings and central spots with strong intensity. In Fig. S10b, we only changed the analyzer to left-handed circular, resulting in blocking out of almost all colorful rings and the central spots. An exception is seen in the lower-hand left-most shell, where the green (5,9) ring can still be seen weakly. This is most likely a result of the ellipticity of the polarization that is Bragg-reflected this far from the shell center being so far from circular, that the employed polarizers are no longer fully adequate, although more complex processes related to subsidiary oscillations may also play a role here [3].

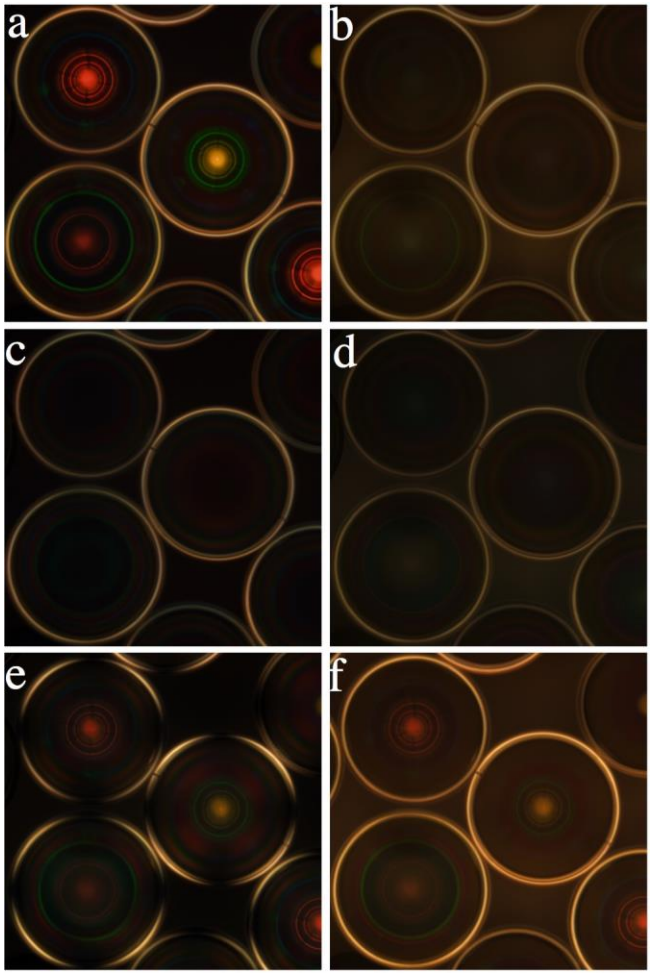

Figure S10: Reflection microscopy images of ChLC shells in different polarization modes: In (a) and (b), the shells are illuminated by right-handed circular polarized light and analyzed by right-handed circular polarizer in (a) and left-handed circular polarizer in (b). In (c) and (d), the shells are illuminated by left-handed circular polarized light and analyzed by left- and right-handed circular polarizer, respectively. In (e) the shells are

between crossed polarizers, whereas (f) is obtained without polarizers. The exposure of photo (b) was unfortunately different from the others, hence the exposure has been digitally adjusted until the background was similar to the other photos.

The outermost white rings remain with roughly similar intensity. This shows that the reflected light of the central spots and rings is indeed right-handed circularly (or elliptically) polarized, i.e. with the same handedness as the cholesteric helix, as expected.

The TIR light along the periphery, in contrast, is linearly polarized, as demonstrated below.

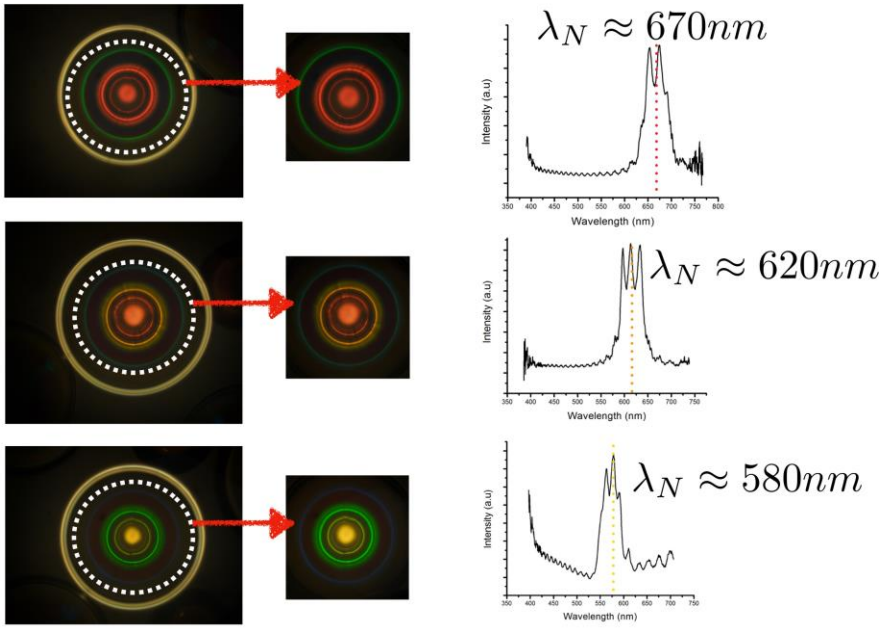

Figure S11: Spectroscopic investigation of the reflections from three representative shells. Unfortunately only the central spot reflections can be recognized clearly in the spectra.

In Fig. S10c-d, the shells are illuminated by left-handed circular polarized light and observed through left- and right-handed circular analyzer, respectively. In both cases, the colorful rings are largely absent, the exception again being the (5,9) ring in the lower left-hand shell, which is still weakly present due to its deviation from perfect circular polarization. Between crossed linear polarizers (e), the reflection patterns are obtained in somewhat lower intensity compared to Fig. S10a, reflecting the fact that a linear polarizer absorbs 50% of circular polarization. The outer white rings now show a strong modulation along the perimeter, with minimum intensity at the extreme horizontal and vertical positions. At these points the shell radius is along the axis of either the

polarizer or the analyzer. The fact that the perimeter is dark at these points shows that the

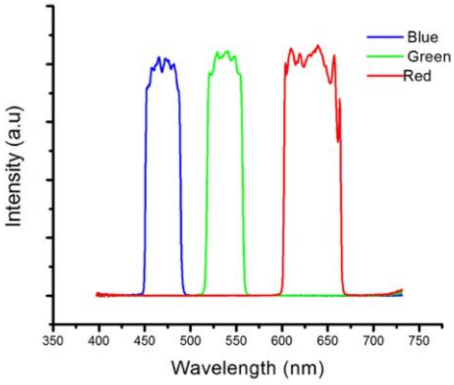

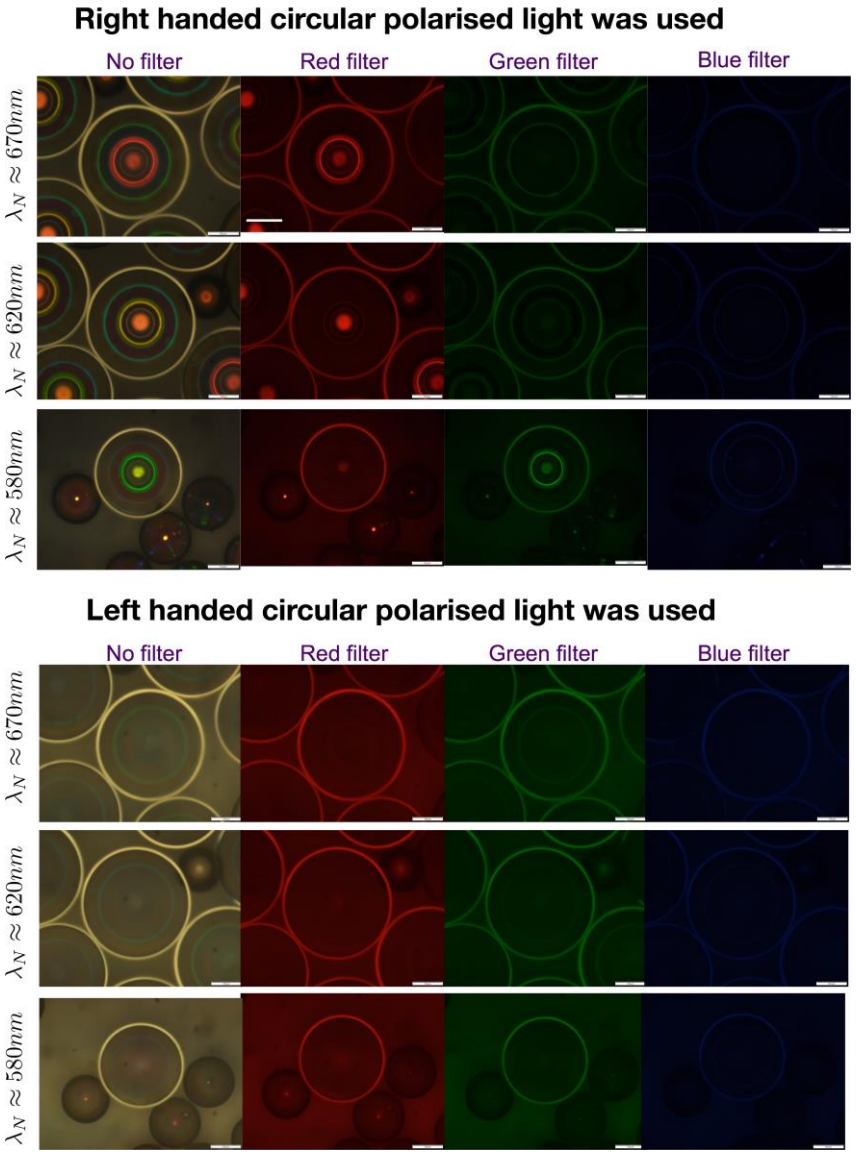

Figure S12: Reflection texture of three representative shells as seen through right- and left-handed circular polarizer, respectively, direct and through red, green and blue filter, respectively. The transmission spectra of the three filters are shown on top.

TIR light experiences birefringence of the ChLC, with the optic axis along the helix axis, as typical for short-pitch cholesterics when light enters more or less perpendicular to the helix.

In Fig. S10f, finally, we observed the shells under natural light illumination without any polarizer. The reflection patterns and the white rings are all visible, but with less sharp features due to scattering and reflection of light from the surroundings, e.g. the glass capillary and other interfaces.

S8 Investigations with spectrophotometer and color filters

We measured the reflection spectra of three representative shells using a spectrometer (Avantes AvaSpec-2048) connected to the polarizing microscope via an optical fiber. The field aperture was closed until the white outermost ring disappeared (arrow between photos). Unfortunately, the intensity of the rings is too weak to recognize them in the spectra, hence only the central spot wavelength can be quantified in this way, see Fig. S11.

We therefore also studied the shells through red, green and blue color filters, respectively, see Fig. S12. This allows us to narrow down the ring wavelengths to the window of the filter with which they are visible. Unfortunately, no interference filters with narrow band gap could be mounted in the reflection path of the optical microscope, hence we had to use filters with rather broad band gap. These are quantified in the transmission spectra at the top of Fig. S12.

S9 SI Movies

S9.1 SI Movie 1

Heating shells of ChLC1 to fully isotropic phase (from 30℃ to 60℃) at 20 K min^{-1} in the tilted microscope. Once the isotropic phase is reached, we hold the temperature and observe the increase in shell asymmetry, becoming much thinner at the top. The movie is in real time.

S9.2 SI Movie 2

Shell production process using a glass capillary microfluidic set-up. Since the production rate is very high, the movie has been slowed down 60 times to allow monitoring of the

details of the shell production. Note how the liquid crystal rotates rapidly in the plane of the capillary immediately after shell release (there may also be a rotation out of plane but this cannot be detected with the standard microscope geometry). S9.3

S9.3 SI Movie 3

Reflection polarizing microscopy (right-handed circular polarizers) of a shell with ChLC1 with green normal-incidence reflection color, while changing the focus, starting from the top and moving to the bottom. By changing focal planes in a shell, we emphasize different rings sequentially, since they arise from reflection events at different vertical levels. With focus close to the shell top or (in particular) bottom, an additional set of weak rings can be seen, probably Grandjean-Cano defect rings generated by the confinement between the inner and outer phases. The movie is real time.

S9.4 SI Movie 4

Lateral translation of a sample with two adjacent shells, observed in reflection with an illumination area that is minimized by fully closing the field aperture. The sequence of appearance/disappearance of the colorful rings, in relation to the illuminated area, confirms that the internal reflection paths give rise to mirror-symmetric reflection patterns in the shells. The movie is real time.

References

1. I. I. Smalyukh, S. Chernyshuk, B. I. Lev, A. B. Nych, U. Ognysta, V. G. Nazarenko, and O. D. Lavrentovich, “Ordered droplet structures at the liquid crystal surface and elastic-capillary colloidal interactions,” Phys. Rev. Lett., vol. 93, no. 11, p. 117801, 2004.
2. A. Utada, E. Lorenceau, D. R. Link, P. D. Kaplan, H. A. Stone, and D. A. Weitz, “Monodisperse double emulsions generated from a microcapillary device,” Science, vol. 308, no. 5721, pp. 537–541, 2005.
3. H. Takezoe, Y. Ouchi, M. Hara, A. Fukuda, and E. Kuze, “Experimental studies on reflection spectra in monodomain cholesteric liquid crystal cells: total reflection, subsidiary oscillation and its beat or sweel structure,” Jap. J. Appl. Phys., vol. 22, no. 7, pp. 1080–1091, 1983.